

Network analysis of mineralogical systems

SHAUNNA M. MORRISON¹, CHAO LIU¹, AHMED ELEISH^{1,2}, ANIRUDH PRABHU²,
CONGRUI LI², JOLYON RALPH³, ROBERT T. DOWNS⁴, JOSHUA J. GOLDEN⁴,
PETER FOX², MICHAEL B. MEYER¹, AND ROBERT M. HAZEN^{1,*}

¹Geophysical Laboratory, Carnegie Institution for Science,

5251 Broad Branch Road NW, Washington, D.C. 20015, U. S. A.

²Tetherless World Constellation, Department of Earth and Environmental

Sciences, Rensselaer Polytechnic Institute, Troy, New York 12180, U. S. A.

³Mindat.org, 128 Mullards Close, Mitcham, Surrey, CR4 4FD, United Kingdom

⁴Department of Geosciences, University of Arizona,

1040 East 4th Street, Tucson, Arizona 85721-0077, U. S. A.

ABSTRACT

A fundamental goal of mineralogy and petrology is the deep understanding of mineral phase relationships and the consequent spatial and temporal patterns of mineral coexistence in rocks, ore bodies, sediments, meteorites, and other natural polycrystalline materials. The multi-dimensional chemical complexity of such mineral assemblages has traditionally led to experimental and theoretical consideration of 2-, 3-, or n -component systems that represent simplified approximations of natural systems. Network analysis provides a dynamic, quantitative, and predictive visualization framework for employing “big data” to explore complex and otherwise hidden higher-dimensional patterns of

diversity and distribution in such mineral systems. We introduce and explore applications of mineral network analysis, in which mineral species are represented by nodes, while coexistence of minerals is indicated by lines between nodes. This approach provides a dynamic visualization platform for higher-dimensional analysis of phase relationships, because topologies of equilibrium phase assemblages and pathways of mineral reaction series are embedded within the networks. Mineral networks also facilitate quantitative comparison of lithologies from different planets and moons, the analysis of coexistence patterns simultaneously among hundreds of mineral species and their localities, the exploration of varied paragenetic modes of mineral groups, and investigation of changing patterns of mineral occurrence through deep time. Mineral network analysis, furthermore, represents an effective visual approach to teaching and learning in mineralogy and petrology.

Keywords: network analysis, igneous petrology, mineral evolution, copper, chromium, phase equilibria, Bowen's reaction series, visualization, big data, cluster analysis, multi-dimensional scaling, education

* E-mail: rhazen@ciw.edu

INTRODUCTION

Network analysis encompasses a powerful array of mathematical and visualization methods that have found numerous applications in the presentation and interpretation of “big data” in varied fields of technology and science (Kolaczyk 2009; Newman 2013). Technological networks include the physical infrastructures of power grids (Pagani and Aiello 2013), roads (Dong and Pentland 2009), and water supply systems (Hwang and Houghtalen 1996; Geem 2010), as well as communications infrastructure (Pinheiro 2011), commercial distribution networks (Guimerá et al. 2005), and the Internet and other information networks (Otte and Rousseau 2002). In the familiar realm of social interactions, networks are used to quantify and visualize data in such diverse topics as the spread of disease, the links among Facebook “friends,” the structure of terrorist organizations, and connections among research collaborators (Otte and Rousseau 2002; Abraham et al. 2010; Scott and Carrington 2011; Kadushin 2012). Network analysis has been applied in biology to the study of ecosystem diversity (Banda et al. 2016), food webs (Martinez 1992; Dunne et al. 2008), neural networks (Müller et al. 1995), biochemical pathways (Costanzo et al. 2016), proteomics (Amital et al. 2004; Harel et al. 2015; Ueza et al. 2016), paleogeography (Sidor et al. 2013; Dunhill et al. 2016; Huang et al. 2016), and evolution (Vilhena et al. 2013; Cheng et al. 2014; Corel et al. 2016). In each of these network applications and more, the modeling, graphing, and analysis of data reveals previously unrecognized patterns and behaviors in complex systems.

Qualitative network-like representations of minerals have been presented previously (e.g., Christy et al. 2016). However, in spite of its utility and widespread application, quantitative network analysis does not appear to have been applied to mineralogical

problems. Here we introduce and apply network analysis to topics in mineralogy and petrology—fields that are especially amenable to this approach because they consider systems of numerous mineral species that co-exist in myriad combinations in varied deposits. In particular, we demonstrate that network analysis of equilibrium mineral assemblages has the potential to elucidate phase relationships in complex multi-dimensional composition space, while revealing previously hidden trends in spatial and temporal aspects of mineral diversity and distribution.

In this contribution we consider varied network representations of three contrasting mineral systems: (1) common rock-forming minerals in intrusive igneous rocks; (2) terrestrial minerals containing the element chromium; and (3) minerals containing the element copper. These subsets of the more than 5200 mineral species approved by the International Mineralogical Association’s Commission on New Minerals and Mineral Names (IMA-CNMMN) exemplify the potential of network analysis to address fundamental questions in mineralogy and petrology.

EXAMPLES OF MINERAL NETWORKS

Minerals, whether in rocks, sediments, meteorites, or ore deposits, exist as assemblages of coexisting species. Here we introduce mineral networks as a strategy to represent and analyze the large and growing data resources related to these assemblages with a variety of mathematical and graphical models—network “renderings” that are available through open access sources. In each case mineral networks employ nodes (also known as vertices), each corresponding to a mineral species. Some node pairs are connected by links (also known as edges), which indicate that those two minerals are

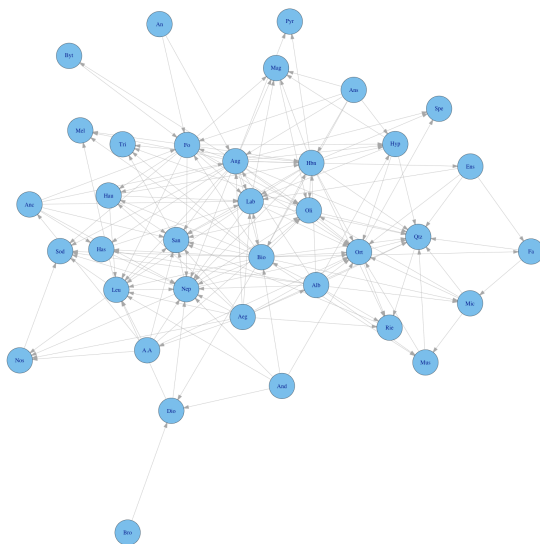
found together. Variations in the ways that nodes and links are represented highlight different aspects of network relationships, as illustrated in the following examples.

Fruchterman-Reingold Force-Directed Networks: Figure 1A illustrates a simplified Fruchterman-Reingold force-directed network (Fruchterman and Reingold 1991; Csardi and Nepusz 2006), representing 36 major rock-forming minerals that occur in holocrystalline intrusive igneous rocks, as described in Alfred Harker’s classic *Petrology for Students* (Harker 1964). Mineralogical descriptions of 77 igneous rocks, each with 1 to 6 major minerals (see Supplemental Information 1), provide the input data for this visualization.

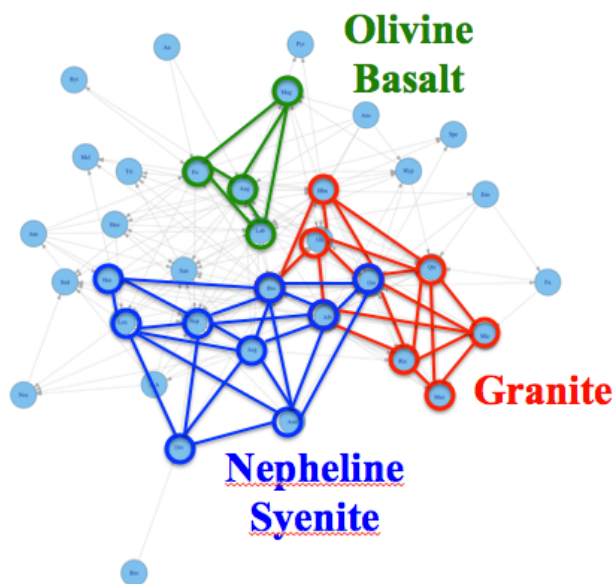
Note that many of the mineral names employed by Harker do not correspond to approved IMA-CNMMN species. In some instances, such as “biotite,” “hornblende,” and “tourmaline,” the names once commonly employed by optical petrologists have been replaced by several related species (i.e., annite, fluorannite, siderophyllite, and tetraferriannite for “biotite”). In the case of plagioclase feldspar, on the other hand, Harker distinguishes six compositional variants—albite, oligoclase, andesine, labradorite, bytownite, and anorthite—as opposed to the two end-member species albite and anorthite recognized as valid species by the IMA-CNMMN.

In Figure 1, we created a simplified Fruchterman-Reingold force directed network using the igraph package in R. We imported tabulated data on coexisting rock-forming minerals into R as a data frame, which was then converted into a matrix object to enable visualization using the igraph package. The igraph software enables a high level of customization based on different network metrics. If “auto.layout” is used, then the

package finds the best-suited algorithm based on the nodes and the number of links
between the nodes. After some preliminary analysis, we found the best-suited algorithm
to be the Fruchterman-Reingold force-directed network with self-loops removed.



A



B

Figure 1. (A) A Fruchterman-Reingold force-directed network diagram of 36 rock-forming minerals in holocrystalline intrusive igneous rocks. Each circular node represents a rock-forming mineral and each link indicates pairs of coexisting minerals in one or more rocks, as recorded in Harker (1964). (B) Different types of igneous rocks appear as closely linked clusters, or “cliques,” in this diagram.

A consequence of these graphical procedures is that each igneous rock type, such as granite, olivine basalt, or nepheline syenite, is embedded as localized, fully interconnected subsets of nodes, or “cliques,” in this network (Figure 1B). For example, the clique for minerals commonly found in granite includes quartz, muscovite, biotite, orthoclase, albite, oligoclase, microcline, hornblende, and riebeckite, whereas olivine basalt contains the clique of labradorite, augite, forsterite, and magnetite. Each of the 77 holocrystalline igneous rocks described by Harker (1964) is similarly embedded in this network. Thus, this visualization in a sense represents the sweep of igneous petrology in a single diagram—a result that hints at the large amount of multi-dimensional information embedded in network representations, while also suggesting a visual opportunity for teaching and learning about rocks and minerals.

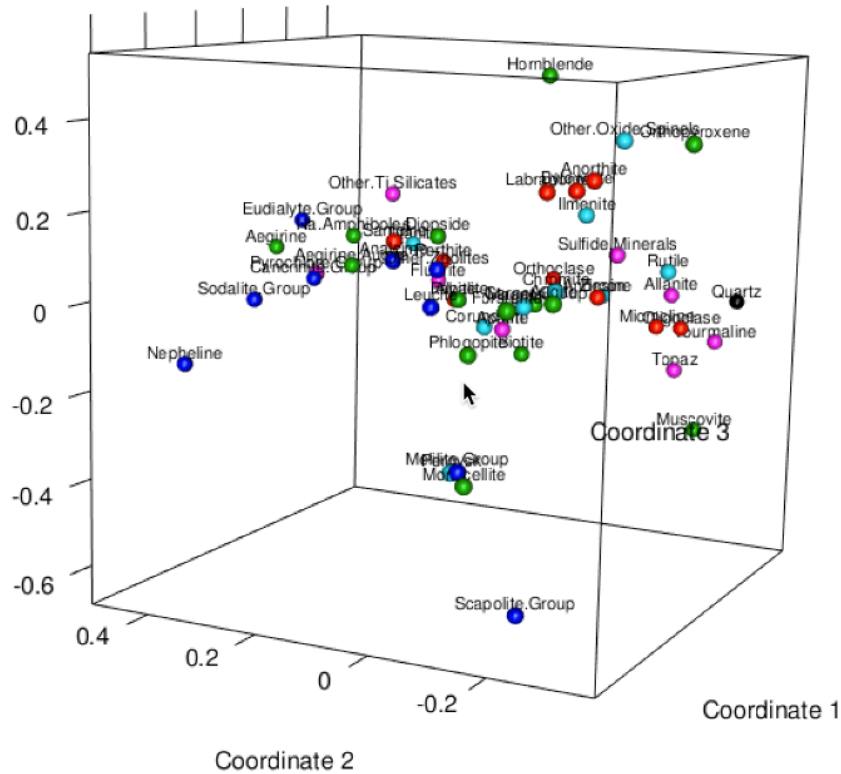
Multi-Dimensional Scaling and Mineral Phase Topologies: A major research objective of mineralogy and petrology for more than a century has been the elucidation of mineral reaction series and phase equilibria (e.g., Bowen 1928; Yoder 1976). We postulate that, because mineral networks are based on observed assemblages of coexisting minerals, they must embed information on phase topologies and thus have the potential to reveal phase relationships in systems not yet studied experimentally.

To illustrate this potential we compiled coexisting mineral data on varied intrusive igneous rocks from *A Descriptive Petrography of the Igneous Rocks* by Albert Johannsen (1932-1938). We consolidated Johannsen’s multi-volume treatment with lists of mineral modes into coexistence data for 51 primary rock-forming minerals in 729 crystalline

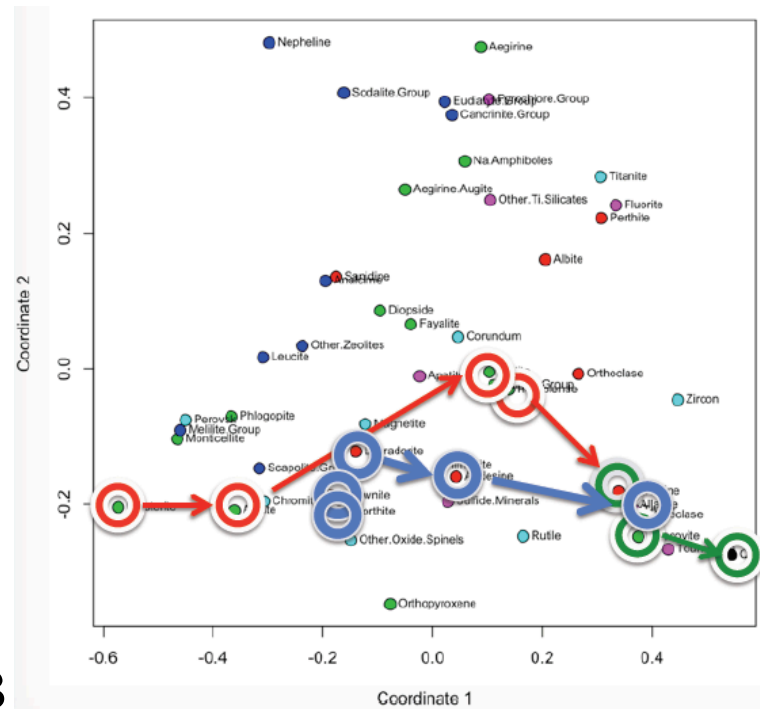
igneous rocks (Supplemental Information 2). We used a variety of mineral network renderings to study the patterns of coexisting phases in these rocks.

We initially employed multi-dimensional scaling in both three- and two-dimensional renderings (<https://github.com/lic10/DTDI-DataAnalysis>; Figures 2 and 3). We created the multi-dimensional scaling diagrams in Figures 2 and 3 using the “cmdscale” command of the “stats” package in R (see <https://github.com/lic10/DTDI-DataAnalysis>). We loaded the Johannsen igneous rock dataset (1932-1938) into R as a data frame, and generated a second data frame as a symmetric 51×51 mineral matrix in which the value recorded at matrix element ij represents the calculated distance, d_{ij} between nodes i and j . Distances were projected on both 2- and 3-dimensional spaces. We used the “rgl” package in R (Adler et al. 2016) to generate the 3D plot. In general, a network containing N nodes requires a representation in $(N - 1)$ dimensions to satisfy exactly all d_{ij} . Consequently, multi-dimensional scaling diagrams of fewer than $(N - 1)$ dimensions employ distance least-squares analysis to distribute nodes as a projection from higher-dimensional space.

Familiar aspects of igneous mineral phase relationships are embedded in the multi-dimensional scaling diagram for igneous minerals. For example, Bowen (1928) proposed a mineral reaction series for igneous rocks in which Mg-Fe minerals tend to crystallize in a mafic cooling sequence (olivine → pyroxene → hornblende → biotite), whereas plagioclase feldspars transition from more calcium-rich to more sodium-rich varieties. At lower temperatures, late-stage minerals display a trend from alkali feldspar to muscovite to quartz. These mineral crystallization trends are mimicked from left-to-right in the multi-dimensional scaling diagram, as illustrated in Figure 2B.



A



B

Figure 2. Multi-dimensional scaling diagrams of 51 rock-forming minerals in 729 igneous rocks tabulated by Johannsen (1932-1938). A. Three-dimensional rendering (see Supplemental Information 3 for animation). B. Two-dimensional rendering with superimposed Bowen's reaction series (Bowen 1928), with the mafic trend (red), plagioclase series (blue), and late-stage trend (green).

In addition, the topology of phase connections in mineral network diagrams mirrors their phase relationships. For example, the “AFQ” ternary phase diagram for the system anorthite ($\text{CaAl}_2\text{Si}_2\text{O}_8$)—forsterite (Mg_2SiO_4)—silica (SiO_2) illustrates that quartz may coexist with anorthite and an intermediate mineral enstatite (MgSiO_3), but not with forsterite (Figure 3A). The topology of this phase diagram is also embedded in the multi-dimensional scaling diagram (Figure 3B).

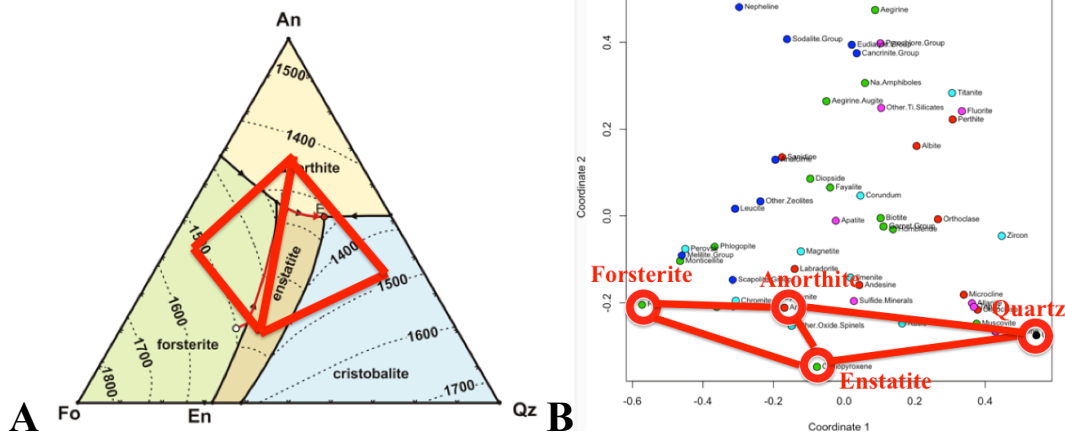


Figure 3. The topologies of phase diagrams, such as the anorthite-forsterite-quartz ternary solidus diagram (A), are mirrored in the topologies of mineral network diagrams (B). Ternary diagram after Anderson (1915).

The phase relationships of igneous rocks have been well documented through decades of studies in experimental petrology and thermochemical modeling, so the examples in Figures 2 and 3 illustrate the conformity of network diagrams to established phase relationships. However, numerous other mineralogical systems have not been investigated in this detail. Much work remains to be done, but we postulate that mineral network analysis of coexisting species in other complex natural chemical systems holds the prospect of revealing unknown phase relationships through multi-dimensional analysis.

Cluster Analysis and Paragenetic Modes: Cluster analysis employs mineral network data to identify subsets of closely related species—an approach that can reveal previously unrecognized relationships among species. For example, we performed cluster analysis on the 30 commonest terrestrial Cr minerals. We included minerals that satisfy three criteria: (1) Cr occupies more than 50% of at least one symmetrically distinct crystal lattice site; (2) the mineral occurs at three or more localities; and (3) the mineral co-occurs with other Cr minerals at two or more localities. In Figure 4 we applied the Walktrap Algorithm (Pons and Latapy 2005) of the igraph package in R to mineral coexistence data in mindat.org to detect clusters of closely related Cr minerals. This approach is based on the analysis of random walks among links. Random walks are more likely to stay within a single cluster because there are more links within a cluster than links leading to different clusters. When we employ this algorithm to perform 5-step random walks on the Cr mineral graph, the minerals separate naturally into four clusters, each of which can be associated with a different paragenetic mode.

A valuable attribute of network diagrams is that the node representations can incorporate additional dimensions of information through their size, color, shape, and patterning. In Figures 4 and 5 if two minerals A and B occur at a and b localities, respectively, and they co-occur at c localities, then the node diameters of A and B are $\log_2(a)$ and $\log_2(b)$, and the distance of the link connecting A and B is $[1 - c/\min(a,b)]$, where $\min(a,b)$ is the smaller of a and b . If A and B always occur together then we assign a minimum distance of 0.1.

These minerals separate naturally into four clusters, the largest of which includes 17 Cr³⁺ minerals, all of which are high-temperature igneous, metamorphic, and

hydrothermal species (group 1). Three additional clusters falling peripherally to this central cluster include all Cr^{6+} minerals, seven of which (group 2) form from low-temperature, oxidized hydrothermal fluids leaching Cr-rich igneous rocks. The remaining six Cr^{6+} minerals, which lie above the central cluster, are sedimentary species found in soils (group 3) and in desert environments (group 4). Cluster analysis is consistent with the observation that chromium in terrestrial Cr^{6+} minerals is probably sourced from Cr^{3+} reservoirs, either through hydrothermal leaching or oxidative weathering (e.g., Liu et al. 2017). We conclude that cluster analysis holds promise for revealing patterns of diagenesis and distribution in a variety of mineral systems.

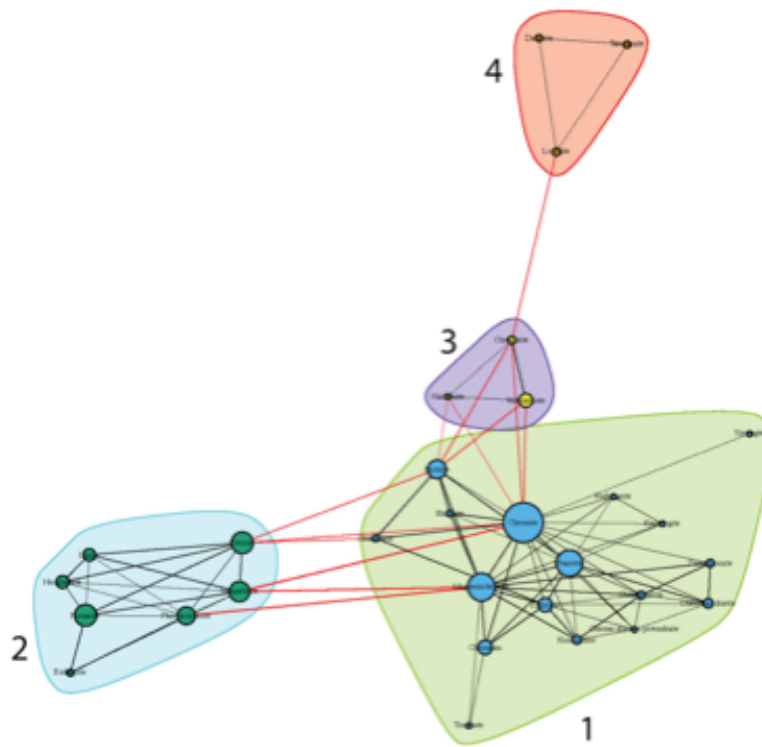


Figure 4. Cluster analysis of 30 common chromium-bearing minerals reveals segregation into 4 groups. The central cluster (group 1) includes 17 Cr^{3+} species formed through igneous, metamorphic, or hydrothermal processes. The left-hand cluster (group 2) includes 7 Cr^{6+} species formed through hydrothermal alteration, whereas the two smaller clusters (groups 3 and 4) include chromate minerals precipitated in soils and desert environments.

Force-Directed Mineral Graphs: An important potential contribution of mineral network analysis lies in the simultaneous visualization and study of relationships among scores or hundreds of minerals that are related by composition, age, tectonic setting, deposit type, or numerous other variables. Force-directed graphs (Figure 5), which represent the distribution of nodes as a dynamic network with balanced spring-like interactions among nodes, are particularly useful in this regard. We generate these graphs by algorithms that run through a number of iterations, displacing the nodes according to fictive attractive and repulsive forces that they exert on each other, until a layout is found that minimizes the “energy” of the system and possibly satisfies other constraints such as drawing connected nodes at certain separations. These methods are implemented in highly customizable modules in multiple programming languages, such as Javascript and R, making it possible to render the graphs through a number of interfaces including web browsers.

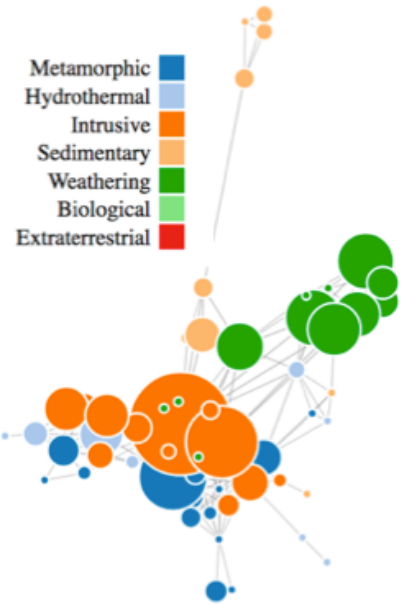
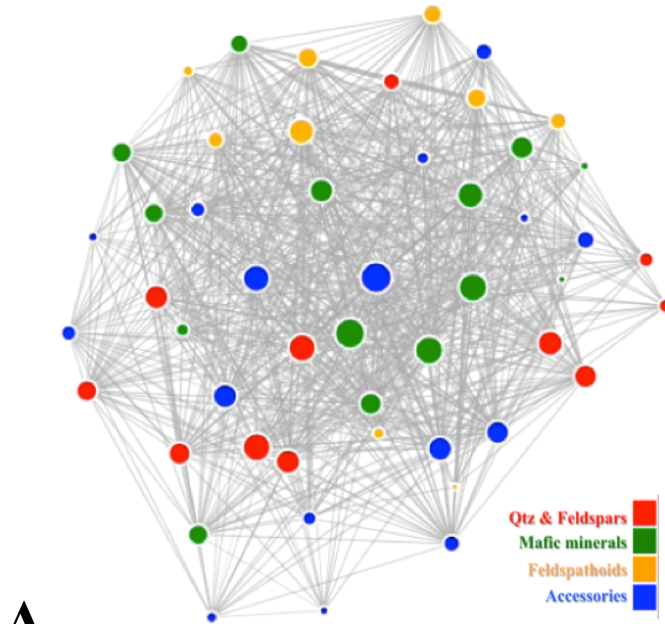
In Figure 5, we created the browser-based force-directed graphs using the D3 4.0 d3-force module, which simulates physical forces using velocity Verlet integration (Verlet 1967) and implements the Barnes–Hut approximation (Barnes and Hut 1986) for performing n -body simulations, similar to those of molecular or planetary systems. For each of the three graphs we compiled a symmetric matrix whose non-diagonal elements represent the number of localities where two minerals coexist and whose diagonal elements represent the total number of localities at which each mineral is found. As a preliminary step we imported these data into R as data frames and converted into two lists, one with nodes representing all the minerals in the dataset, and the other with links representing coexistence relationships between the nodes. We

created the list of nodes by extracting the row or column names of the data frame, each of which represents a mineral, and we produced the list of links by iterating over the upper or lower triangle of the matrix and copying the row name, column name, and computing a coexistence metric between the two minerals. We added additional fields to the nodes list, such as mineral compositions, the number of localities at which the mineral occurs, and/or structural classification of the mineral.

We combined these two lists and converted them into a JSON (Javascript Object Notation) file, which is stored along with a web page written in HTML (Hypertext Markup Language) and Javascript that uses functions from the D3 4.0 library. The data file is read from the file system and rendered when the page is opened in a web-browser. Our Javascript code generates the layout by performing a many body (n -body) simulation and constraining edge lengths to values that equal the coexistence metric multiplied by a constant to make the connections more apparent. We set node sizes to the binary logarithm of the abundance value of a mineral in the cases of Cu and igneous rocks diagrams, and the actual abundance values in the Cr diagram. Node colors in Figure 5 variously indicate the structural classification of the minerals (igneous network), paragenetic mode (Cr network), and composition (Cu network).

The mineral network diagrams in this study require data on coexisting minerals in individual rocks or from individual localities. We manually generated spreadsheets of coexisting minerals in igneous rocks from text and tables in Harker (1964) and Johannsen (1932-1938) as presented in Supplemental Information 1 and 2. We used a PERL script to construct spreadsheets of coexisting chromium and copper minerals, which are generated automatically from data on coexisting species from localities

recorded in the crowd-sourced mineral website mindat.org. We define Cr- or Cu- minerals as those reported in the official IMA list of minerals at ruff.info/ima. For each pair of coexisting minerals we generated a file that contains all localities at which those two minerals occur. A second program reads the assembled files to obtain the number of localities at which each pair occurs and outputs these counts in matrix form.



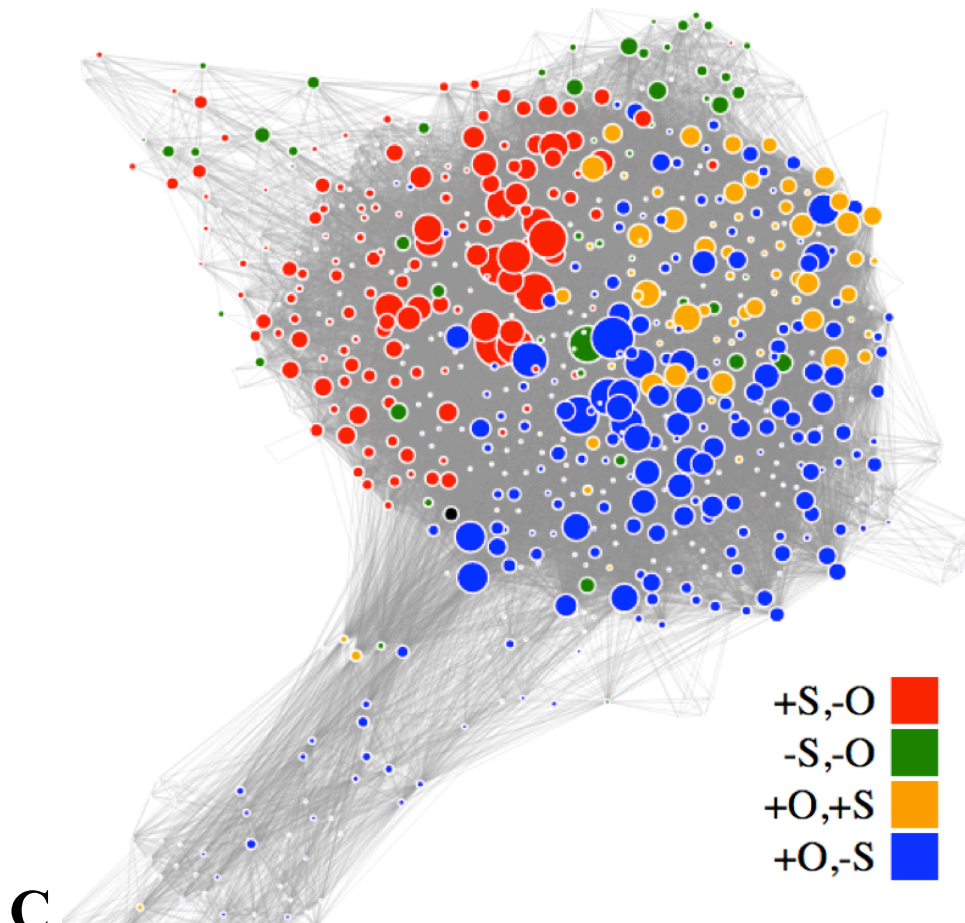


Figure 5. Force-directed network graphs of minerals. A. 51 rock-forming igneous minerals sorted by structural groups. B. 58 chromium minerals sorted by paragenetic mode. C. 664 copper minerals sorted by composition. See Supplemental Information 4, 5, and 6, respectively, for animations of these three dynamic graphs.

An important feature of browser-based force-directed graphs is that they can be manipulated with a mouse—individual nodes can be “pulled aside,” thus deforming the network and illustrating the number and nature of links to other nodes (see movies in Supplemental Information 4, 5, and 6). Figure 5 presents static images of three contrasting force-directed graphs: (1) 51 common rock-forming igneous minerals; (2) 58 terrestrial minerals of chromium; and (3) 664 minerals of copper.

In Figure 5A, which represents connections among 51 igneous minerals, the node colors indicate broad compositional groups (see figure for key). Note that while colors are largely mixed, the red (quartz and feldspar minerals) and orange (feldspathoids and zeolite mineral) nodes tend to concentrate near the lower and upper halves of the network, respectively—a feature that reflects the natural avoidance of quartz and feldspathoids. Node colors in Figure 5B for chromium minerals correspond to paragenetic modes; note the strong clustering of nodes by color—an observation that parallels the cluster analysis in Figure 4. Node colors in Figure 5C for copper minerals indicate mineral compositions separated according to the presence or absence of sulfur or oxygen. Strong segregation by color reveals clustering according to these compositional variables for sulfides, sulfates, and oxygen-bearing species.

Network metrics: An important attribute of networks is the ability to compare and contrast their topological characteristics through the use of many quantitative network metrics (e.g., Newman 2013; Table 1). For example, a network's edge density D , defined as the ratio of the number of observed links to the maximum possible number of links, quantifies the extent to which a network is interconnected. For a network with N nodes and L links:

$$D = 2L/[N(N - 1)]. \quad \text{[Equation 1]}$$

D can vary from 0 in a network with no links to 1 for a fully connected network. For mineral networks, 0 means every mineral occurs by itself, whereas 1 means every mineral co-occurs with every other mineral.

Freeman network centralization or degree centralization, FNC , is one of several measures of how many nodes play central roles in the network. In a network of N nodes, degree centralization for each node i is the number of links to other nodes, or node degree, $\deg(i)$. Freeman network centralization is defined as:

$$FNC = \sum_{i=1}^N \frac{\deg_{\max} - \deg(i)}{(N-1)(N-2)}, \quad [\text{Equation 2}]$$

in which \deg_{\max} is the maximum degree node. FNC can vary from 0 to 1; in a mineral network, low centralization indicates that minerals are uniformly interconnected, whereas high centralization indicates that only one or a few minerals are highly connected.

Transitivity, T , is defined by the ratio of the number of loops of length three and the number of paths of length two in a network. In mineral networks, 0 means that minerals co-occur only as pairs and 1 means that each mineral co-occurs with at least two others.

Diameter, d , of a network with N nodes is defined as the maximum value of the shortest path (i.e., “degree of separation”) between any two nodes in the network, as determined by the number of edges and the average edge length between the two nodes.

Mean distance, MD , of a network with N nodes indicates the average path length, calculated from the shortest paths between all pairs of nodes. In a mineral network, MD represents the average separation between mineral pairs.

The three force-directed mineral networks illustrated in Figure 5 differ significantly in their network metrics. The igneous mineral network (Figure 5A) is relatively dense with high transitivity ($D = 0.64$; $T = 0.77$), while the network is decentralized ($FNC = 0.34$), and compact ($d = 1.1$; $MD = 1.36$). Two minerals, biotite and magnetite, have links to all other minerals; thus, manipulating the nodes for biotite and magnetite (see movie in Supplemental Information 4) results in a rapid return to the initial equilibrium network

configuration with those nodes appearing near the center of the network. Manipulation of quartz (near the bottom of the network) and nepheline (near the top), by contrast, illustrates the avoidance of those two minerals, which do not co-occur in igneous rocks. We postulate that the relatively high density and low diameter of this network are manifestations of high-temperature equilibrium associated with intrusive igneous rocks, for which a relatively few common rock-forming minerals occur in several lithologies.

Table 1. Network metrics for force-directed graphs (see Figure 5)

Mineral System	Density	Centralization	Transitivity	Diameter	Mean Distance
Igneous minerals	0.64	0.34	0.77	1.1	1.36
Cr minerals	0.05	0.33	0.44	6.0	2.65
Cu minerals	0.12	0.68	0.48	4.0	1.93

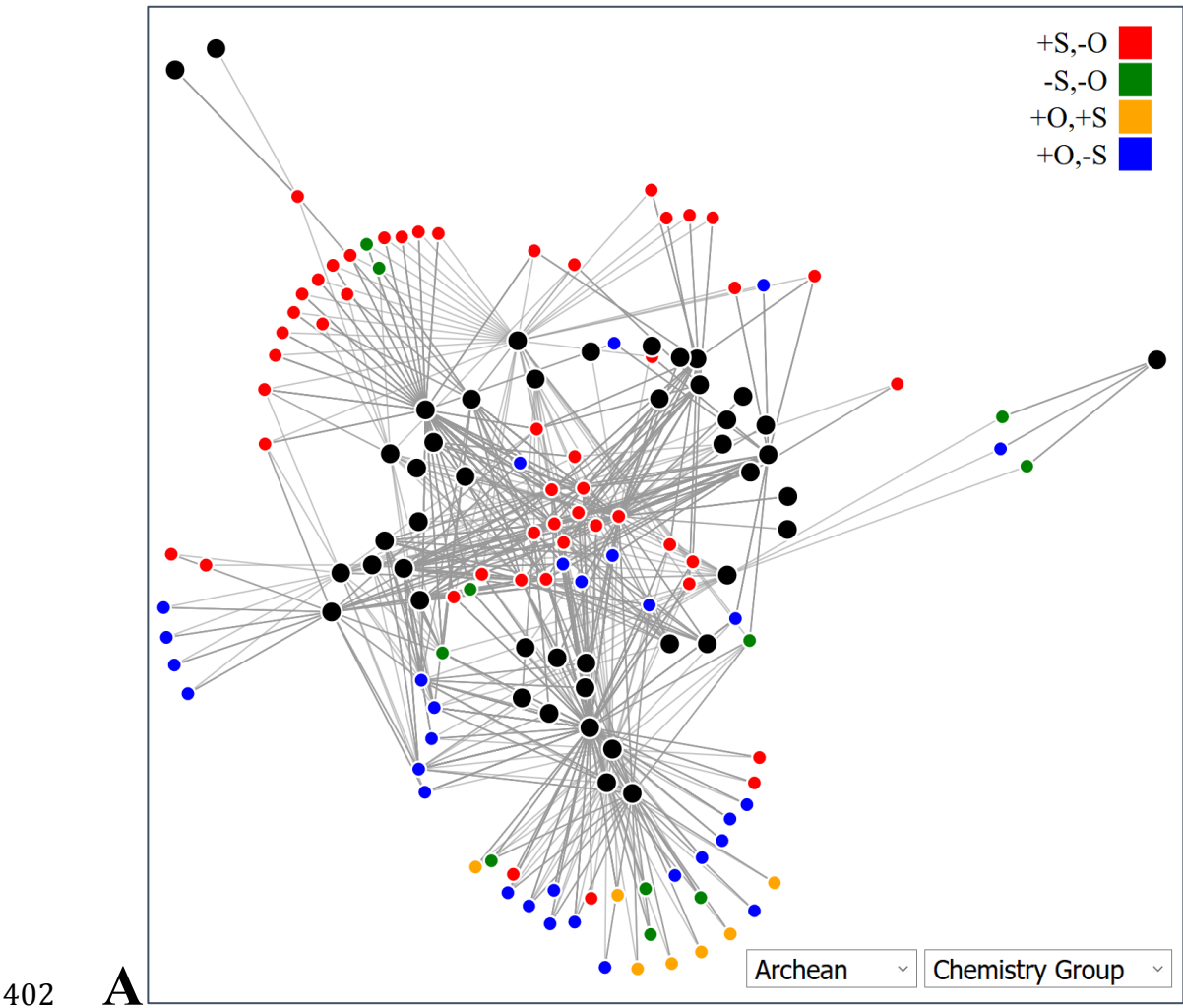
The network for 58 terrestrial chromium minerals (Figure 5B) contrasts with that for igneous minerals in that it possesses much lower density and transitivity ($D = 0.05$; $T = 0.48$), relatively low centrality ($C = 0.33$), and greater diameter and mean distance ($d = 6$; $MD = 2.65$). These values are consistent with the cluster analysis (Figure 4), which revealed four groups of minerals that are largely separate from each other. A striking feature of this Cr mineral network is the segregation of nodes by colors, which represent paragenetic modes (see figure caption). As revealed by cluster analysis, chromium minerals occurring through weathering, formed during metamorphism, found in sediments, or crystallized through igneous processes tend not to co-occur and thus appear as somewhat isolated clusters in Figure 5B. On the other hand, hydrothermal Cr minerals are much more interconnected with phases formed through other paragenetic processes.

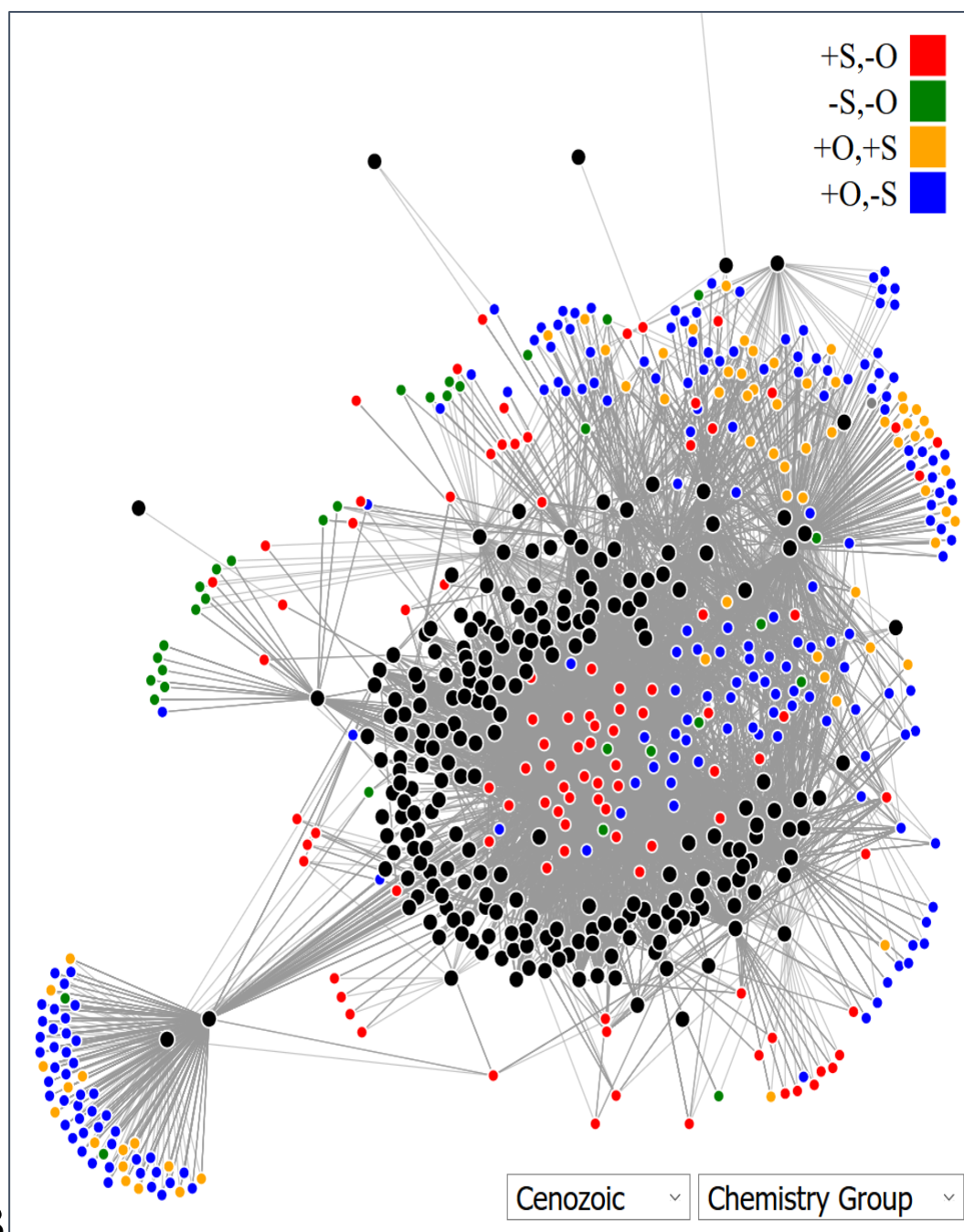
Such complex relationships among 58 minerals become obvious through manipulation of a force-directed graph (see movie in Supplemental Information 5) and exemplify the wealth of information contained in these network diagrams.

Copper minerals (Figure 5C) provide a third, contrasting example of a mineral network with relatively low density and transitivity ($D = 0.12$; $T = 0.44$), high centrality ($FNC = 0.68$), and intermediate diameter and mean distance ($d = 4$; $MD = 1.93$). Aspects of the co-existence of copper minerals are revealed in Figure 5C, which is colored according to the presence or absence of the two principal anions, O and S. A strong degree of segregation is seen for sulfides (red), sulfates (orange), and minerals with O but not S (blue). By contrast, copper minerals with neither O nor S (green) are much more widely distributed, as they are found associated with a variety of other copper minerals. Manipulations of the nodes for the two most interconnected copper minerals, chalcopyrite and malachite, reveal connections to all regions of the graph and result in significant distortion of the entire network (Supplemental Information 6). Manipulation of the node for native copper, on the other hand, shows greater connectivity to oxides and sulfates than to sulfides—an insight not readily obvious from tables of coexisting mineral species (and a finding that will be explored in more detail in a forthcoming study). The ability to view and interrogate simultaneously and dynamically the relationships among hundreds of mineral species underscores the power of force-directed mineral network visualizations.

Bipartite Networks: Bipartite networks incorporate two types of nodes and thus reveal information complementary to the previous examples (e.g., Asratian et al. 1998). Of

394 special interest in mineralogy are network diagrams that include nodes for both mineral
395 species and their localities, with links connecting localities to mineral species found at
396 those localities. In Figures 6A and 6B we present bipartite networks for copper minerals
397 for two contrasting geological time intervals, from the Archean Eon (4.0 to 2.5 Ga) and
398 the Cenozoic Era (543 Ma to present), respectively. We color mineral nodes according to
399 mineral compositions with respect to the presence or absence of oxygen and sulfur, as in
400 Figure 5C. Locality nodes, which in this case represent countries or broad geographic
401 regions, appear in black.





B

Figure 6. Bipartite networks for copper minerals from the Archean Eon (A) and Cenozoic Era (B) reveal distinctive patterns of mineral diversity and distribution through space and time. Black nodes represent localities, whereas colored nodes represent mineral species linked to those localities. The distinctive pattern of an “O” or “U”-shape arrangement of localities with relatively few common minerals in the center area and a greater number of rare minerals in peripheral positions conforms to a Large Number of Rare Events frequency distribution (Hazen et al. 2015; Hystad 2015). Note also the increase in mineral diversity, as well as the evolution of mineral compositions, from A to B.

412
413 As with the previously demonstrated force-directed mineral networks, we employed
414 mineral/locality data to produce the bipartite graphs. We imported data into R where two
415 sets of nodes were extracted, one containing mineral species and the other containing the
416 localities where these minerals occur. We combined the two sets of nodes into one list
417 and added an attribute to each item in the list, determining its type as either mineral or
418 locality. We then generated a list of links from the data such that each link connects a
419 mineral species to a locality. Following the same procedure as with the force-directed
420 graphs created using the D3 4.0 library, we combined the data structures representing the
421 nodes and links into a JSON file linked to an HTML page such that the diagrams can be
422 rendered and manipulated in a web browser.

423 These striking bipartite networks provide simultaneous visual representations of data
424 on the diversity and abundances of mineral species, as well as their geographical
425 distributions, compositional characteristics, and geological ages. As such, these diagrams
426 demonstrate the potential of network analysis to reveal previously unrecognized aspects
427 of mineral evolution and mineral ecology. Insights from these visualizations include:

- 428 • In both networks the nodes of the force-directed graph self-organize into a
429 distinctive pattern with black locality nodes forming an “O” or “U”-shape
430 arrangement. The commoner minerals, those found at numerous localities, appear
431 as colored nodes near the center of these diagrams, whereas a significantly greater
432 number of rare minerals that occur at only one or two localities plot as colored
433 nodes in clusters and “fans” of minerals arranged around the periphery of the
434 diagram. This unanticipated elegant geometry is the visual manifestation of a

435 Large Number of Rare Events (LNRE) frequency distribution that characterizes
 436 Earth's near-surface mineralogy (Hazen et al. 2015; Hystad et al. 2015).

- 437 • The Archean bipartite network (Figure 6A), with 97 Cu minerals from 45 broad
 438 geographical localities, reveals that sulfide minerals dominated copper
 439 mineralogy prior to the Great Oxidation Event (e.g., Hazen et al. 2008; Canfield
 440 2014; Lyons et al. 2014). Sulfides represent 17 (74%) of the 23 common Archean
 441 copper minerals located “inside” the ring of black locality nodes and 32 (50%) of
 442 the 64 rare minerals located around the periphery. Note also the relative paucity of
 443 sulfate minerals—only 7 species (7%), all of them rare, out of 97 Archean copper
 444 minerals.
- 445 • The Cenozoic bipartite network for copper minerals contrasts with that of the
 446 Archean Eon in a number of respects. The significant increase in the number of
 447 identified mineral species (colored nodes), from 97 to almost 400, is to be
 448 expected when comparing Earth's recent mineralogy with the scant record of
 449 rocks more than 2.5 billion years old. However, there are also striking and
 450 previously unrecognized differences in the distributions of mineral compositions
 451 from these two geological intervals. Sulfide minerals (red nodes) continue to
 452 make up a significant fraction of common species located near the center of the
 453 diagram. Of the approximately 100 mineral nodes located within the “U” of black
 454 locality nodes, more than 40 are sulfide minerals. Furthermore, most of these
 455 phases are concentrated at the “bottom” of the “U”—a position representing the
 456 most widely distributed copper minerals. Of the remaining common Cu phases in
 457 the central region, most are carbonate, phosphate, and other minerals that contain

oxygen but not sulfur (blue nodes concentrated in the “upper” region inside the “U”), perhaps reflecting the oxygenation by photosynthesis of Earth’s atmosphere and oceans.

- Peripheral (i.e., rare) copper minerals from the Cenozoic Era differ markedly in composition from those of the Archean Eon. Sulfide minerals account for only about 50 (<20%) of the more than 280 rare species, whereas at least 210 (~75%) oxygen-bearing minerals, 60 of them sulfates, decorate the diagram in sprays and clusters of phases known from only one or two geographic regions.

These intriguing insights regarding copper mineral evolution and ecology have been hidden among large data tables of more than 600 species from more than 10,000 localities, representing more than 100,000 individual mineral-locality data (ruff.info/ima; mindat.org). Research now in progress will investigate these intriguing trends for copper mineral evolution and ecology in greater detail.

CONCLUSIONS

Network analysis provides mineralogists and petrologists with a dynamic, multi-dimensional, quantitative visualization approach to explore complex and otherwise hidden patterns of diversity and distribution in systems of numerous minerals—information that heretofore has been buried in large and growing mineral data resources. Open access data repositories now document more than 5200 mineral species (ruff.info/ima), from 275,000 localities, incorporating approximately one million mineral/locality data (mindat.org). It is thus possible to employ mineral network visualizations to investigate quantitatively patterns of coexistence, phase relationships,

481 reaction pathways, network metrics, frequency distributions, and deep-time evolution of
482 virtually any mineral group.

483 We suggest that further investigation of mineral networks will reveal previously
484 hidden patterns of species coexistence and clustering based, for example, on structure
485 type, chemistry, age, hardness and other mechanical properties, redox state, depth and
486 temperature of formation, and paragenetic mode. Mineral metadata, furthermore, permit
487 exploration of mineral subsets through filtering by geographic region, tectonic setting,
488 co-occurrence with varied biozones, economic resources, environmental characteristics,
489 and other key parameters. In addition, networks are now being generated for minerals on
490 Mars, the Moon, and Vesta (as represented by “HED” achondrite meteorites) with the
491 motivation to compare and contrast mineral evolution and ecology of different planets
492 and moons.

493 Given the inherent beauty and richness of these visualization tools, it is perhaps easy
494 to become distracted from the varied, multi-dimensional, and as yet unexplored aspects of
495 mineralogy that networks promise to illuminate. We look to a future when the
496 consolidated network of all 5200 mineral species, distributed among hundreds of
497 thousands of localities, will offer an unparalleled research tool. We conclude that mineral
498 network analysis, by combining the potential of big data mineralogy with a dynamic and
499 accessible visual aesthetic, represents a powerful new method to explore fundamental
500 problems in mineralogy and petrology.

ACKNOWLEDGEMENTS

We thank Alex Pires and Daniel Hummer for help in database development and Sophie Kolankowski, Benno Lee, Marshall X. Ma, Han Wang, Stephan Zednik, and Hao Zhong for assistance in the development of varied visualization methods. Craig Schiffries and two anonymous reviewers provided thoughtful comments and suggestions. This work was supported by the W. M. Keck Foundation's Deep-Time Data Infrastructure project, with additional support by the Deep Carbon Observatory, the Alfred P. Sloan Foundation, a private foundation, the Carnegie Institution for Science, and NASA NNX11AP82A, Mars Science Laboratory Investigations. Any opinions, findings, and conclusions or recommendations expressed in this material are those of the authors and do not necessarily reflect the views of the National Aeronautics and Space Administration.

REFERENCES

- Abraham, A., Hassanien, A.-E., and Snasel, V. [Editors] (2010) Computational Social Network Analysis: Trends, Tools and Research Advances. Springer, New York.
- Adler, D, et al. (2016). rgl: 3D Visualization Using OpenGL. R package version 0.95.1441. <http://CRAN.R-project.org/package=rgl>
- Amital, G., Shemesh, A., Sitbon, E., Shklar, M., Netanel, D., Venger, I., and Pietrokovski, S. (2004) Network analysis of protein structures identifies functional residues. *Journal of Molecular Biology*, 344, 1135-1146.
- Anderson, O. (1915) The system anorthite-forsterite-silica. *American Journal of Science*, 39, 407-454.
- Asratian, A.S., Denley, T.M.J., and Häggkvist, R. (1998) Bipartite Graphs and their Applications. Cambridge University Press, New York.
- Banda-R, K. et al. (2016) Plant diversity patterns in neotropical dry forests and their conservation implications. *Science*, 353, 1383-1387.
- Barnes, J. and Hut, P. (1986) A hierarchical $O(N \log N)$ force-calculation algorithm. *Nature*, 324, 446-449.
- Bowen, N.L. (1928) The Evolution of the Igneous Rocks. Princeton University Press, New Jersey.
- Canfield, D. (2014) Oxygen: A Four-Billion Year History. Princeton University Press, New Jersey.
- Cheng, S., Karker, S., Baptiste, E., Yee, N., Falkowski, P., and Bhattacharya, D. (2014) Sequence similarity network reveals the imprints of major diversification events in the evolution of microbial life. *Frontiers in Ecology and Evolution*, 2, 72. Doi:

10.3389/fevo.2014.00072

Christy, A.G., Mills, S.J., Kampf, A.R., Houseley, R.M., Thorne, B., and Marty, J. (2016)

The relationship between mineral composition, crystal structure and paragenetic sequence: the case of secondary Te mineralization at the Bird Nest druft, Otto Mountain, California, USA. *Mineralogical Magazine*, 80, 291-310.

Corel, E., Lopez, P., Méheust, R., and Bapteste, E. (2016) Network-thinking: Graphs to analyze microbial complexity and evolution. *Trends in Microbiology*, 24, 224-237. DOI: 10.1016/j.tim.2015.12.003

Costanzo, M. et al. (2016) A global genetic interaction network maps a wiring diagram of cellular function. *Science*, 353, 1381.

Csardi, G. and Nepusz, T. (2006) The igraph software package for complex network research. *InterJournal, Complex Systems*, 1695, 1-9.

Dong, W. and Pentland, A. (2009) A network analysis of road traffic with vehicle tracking data. In *Proceedings of the American Association of Artificial Intelligence, Spring Symposium, Human Behavior Modeling*, Palo Alto CA, pp.7-12.

Dunhill, A.M., Bestwick, J., Narey, H., and Sciberras, J. (2016) Dinosaur biogeographical structure and Mesozoic continental fragmentation: A network-based approach. *Journal of Biogeography*. doi: 10.1111/jbi.12766 (in press).

Dunne, J.A., Williams, R.J., Martinez, N.D., Wood, R.A., and Erwin, D.H. (2008) Compilation and network analysis of Cambrian Food webs, *PLoS Biology*, 6, 693-708.

Fruchterman, T.M.J. and Reingold, E.M. (1991) Graph drawing by force-directed placement. *Software: Practice and Experience*, 21, 1129-1164.

562 Geem, Z.W. (2010) Optimal cost design of water distribution networks using harmony
563 search. *Engineering Optimization* 38, 259-277.

564 Guimerá, R., Mossa, S., Turschi, A., and Amaral, L.A.N. (2005) The worldwide air
565 transportation network: anomalous centrality, community structure, and cities' global
566 roles. *Proceedings of the National Academy of Sciences USA*, 102, 7794-7799.

567 Harel, A., Karkar, S., Cheng, S., Falkowski, P.G., and Bhattacharya, D. (2015)
568 Deciphering primordial cyanobacterial genome functions from protein network
569 analysis. *Current Biology*, 25, 628-634.

570 Harker, A. (1964) *Harker's Petrology for Students*, 8th edition, revised. Cambridge
571 University Press, New York.

572 Hazen, R.M., Papineau, D., Bleeker, W., Downs, R.T., M., J., McCoy, T.L., Sverjensky,
573 D.A., and Yang, H. (2008) Mineral evolution. *American Mineralogist*, 93, 1693-1720.

574 Hazen, R.M., Grew, E.S., Downs, R.T., Golden, J., and Hystad, G. (2015) Mineral
575 ecology: Chance and necessity in the mineral diversity of terrestrial planets. *Canadian*
576 *Mineralogist*, 53, 295-323. DOI: 10.3749/canmin.1400086.

577 Huang, B., Zhan, R.-B., and Wang, G.-X. (2016) Recovery brachiopod associations from
578 the lower Silurian of South China and their paleoecological implications. *Canadian*
579 *Journal of Earth Science*, 53, 674-679.

580 Hwang, N. and Houghtalen, R. (1996) *Fundamentals of Hydraulic Engineering Systems*.
581 Prentice Hall, Upper Saddle River, New Jersey.

582 Hystad, G., Downs, R.T., and Hazen, R.M. (2015) Mineral frequency distribution data
583 conform to a LNRE model: Prediction of Earth's "missing" minerals. *Mathematical*
584 *Geosciences*, 47, 647-661.

585 Johannsen, A. (1932-1938) A Descriptive Petrography of the Igneous Rocks: 4 Volumes.
 586 University of Chicago Press, Illinois.
 587 Kadushin, C. (2012) Understanding Social Networks. Oxford University Press, New
 588 York.
 589 Kolaczyk, E.D. (2009) Statistical Analysis of Network Data. Springer, New York.
 590 Liu, C., Hystad, G., Golden, J.J., Hummer, D.R., Downs, R.T., Morrison, S.M., Grew,
 591 E.S., and Hazen, R.M. (2017) Chromium mineral ecology. American Mineralogist, in
 592 press.
 593 Lyons, T.W., Peinhard, C.T., and Planavsky, N.J. (2014) The rise of oxygen in Earth's
 594 early ocean and atmosphere. Nature, 506, 307-314.
 595 Martinez, N.D. (1992) Constant connectance in community food webs. American
 596 Naturalist, 139, 1208-1212.
 597 Müller, B., Reinhardt, J., and Strickland, M.T. (1995) Neural Networks: An Introduction.
 598 2nd Edition. Springer, New York.
 599 Newman, M.E.J. (2013) Networks: An Introduction. Oxford University Press, New York.
 600 Otte, E. and Rousseau, R. (2002) Social network analysis: a powerful strategy, also for
 601 the information sciences. Journal of Information Science, 28, 441-453.
 602 Pagani, G.A. and Aiello, M. (2013) The power grid as a complex network: A survey.
 603 Physica A, 392, 2688-2700.
 604 Pinheiro, C.A.R. (2011) Social Network Analysis in Telecommunications. Wiley,
 605 Hoboken, New Jersey.
 606 Pons, P, and Latapy, M. (2005) Computing communities in large networks using random
 607 walks. International Symposium on Computer and Information Sciences. Springer,

New York.

Scott, J. and Carrington, P.J. (2011) The SAGE Handbook of Social Network Analysis.

SAGE: Los Angeles, California.

Sidor, C.A., Vilhena, D.A., Angielczyk, K.D., Huttenlocker, A.K., Nesbitt, S.J., Peacock,

B.R., Steyer, J.S., Smith, R.M.H., and Tsuji, L.A. (2013) Provincialization of

terrestrial faunas following the end-Permian mass extinction. *Proceedings of the*

National Academy of Sciences USA, 110, 8129–8133. doi: 10.1073/pnas.1302323110.

Uezu, A., Kanak, D.J., Bradshaw, T.W.A., Soderblom, E.J., Catavero, C.M., Burette,

A.C., Weinberg, R.J., and Soderling, S.H. (2016) Identification of an elaborate

complex mediating postsynaptic inhibition. *Science*, 353, 1123-1128.

Verlet, L. (1967) Computer "Experiments" on Classical Fluids. I. Thermodynamical

Properties of Lennard-Jones Molecules. *Physical Review*, 159, 98-103.

Vilhena, D.A., Harris, E.B., Bergstrom, C.T., Maliska, M.E., Ward, P.D., Sidor, C.A.,

Strömberg, C.A.E., and Wilson, G.P. (2013) Bivalve network reveals latitudinal

selectivity gradient at the end-Cretaceous mass extinction. *Science Reports*, 3. doi:

10.1038/srep01790.

Yoder, H.S. Jr (1976) Generation of Basaltic Magma. National Academy of Sciences

Washington DC.

Supplemental Information

Supplemental Information Contains:

1. Excel file of 36 minerals from 76 intrusive igneous rocks, as extracted from Harker (1964).
2. Excel file of 51 minerals from 725 intrusive igneous rocks, as extracted from Johannsen (1932-1938).
3. Movie of the rotation of the 3-dimensional multi-dimensional scaling diagram of rock-forming minerals in intrusive igneous rocks.
4. Movie of the manipulation of nodes for biotite, magnetite, quartz, and nepheline in the force-directed graph of intrusive igneous minerals.
5. Movie of the manipulation of nodes for chromite and crocoite in the force-directed graph of terrestrial chromium minerals.
6. Movie of the manipulation of nodes for chalcopyrite, malachite, and copper in the force-directed graph of the 242 most common copper minerals (≥ 50 localities).